



Published in final edited form as:

*Nanomedicine*. 2008 March ; 4(1): 57–69.

## Fabrication of $\{^{198}\text{Au}^0\}$ radioactive composite nanodevices and their use for nano-brachytherapy

Mohamed K. Khan, M.D., Ph.D.<sup>1</sup>, Leah D. Minc, Ph.D.<sup>2</sup>, Shraddha S. Nigavekar, Ph.D.<sup>3</sup>, Muhammed S. T. Kariapper, Ph.D.<sup>1</sup>, Bindu M. Nair, Ph.D.<sup>1</sup>, Matthew Schipper, Ph.D.<sup>2</sup>, Andrew C. Cook, Ph.D.<sup>4</sup>, Wojciech G. Lesniak, Ph.D.<sup>1</sup>, and Lajos P. Balogh, Ph.D.<sup>1</sup>

<sup>1</sup>*NanoBiotechnology Center at RPCI, Department of Radiation Medicine, Roswell Park Cancer Institute, Elm and Carlton Streets, Buffalo, NY 14263*

<sup>2</sup>*OSU Radiation Center, Oregon State University, Corvallis OR, 97331*

<sup>3</sup>*Department of Radiation Oncology, University of Michigan Medical Center, 1500 E. Medical Center Drive, Ann Arbor, MI 48109*

<sup>4</sup>*Department of Nuclear Engineering, Burlington Engineering Laboratories, NC State University, Raleigh, NC, USA 27695-7909*

### Abstract

We describe the simple fabrication of poly( $\{^{198}\text{Au}\}$ ) radioactive gold/dendrimer composite nanodevices in distinct sizes (between  $d=10$  nm and 29 nm) for targeted radiopharmaceutical dose delivery to tumors in vivo. Irradiation of aqueous solutions of  $^{197}\text{Au}$  containing poly(amidoamine) dendrimer tetrachloroaurate salts or  $\{^{197}\text{Au}^0\}$  gold/dendrimer nanocomposites in a nuclear reactor resulted in the formation of positively charged and soluble poly $\{^{198}\text{Au}^0\}$  radioactive composite nanodevices (CNDs). A mouse melanoma tumor model was used to test the poly $\{^{198}\text{Au}^0\}$  CNDs whether they can deliver a therapeutic dose. A single intratumoral injection of poly $\{^{198}\text{Au}^0\}_{d=22\text{nm}}$  CNDs in PBS delivering a dose of 74 microCi, after eight days, resulted in a statistically significant 45% reduction in tumor volume, when compared to untreated groups and those injected with the “cold” nanodevice. No clinical toxicity was observed during the experiments. This study provides the first proof of principle that radioactive composite nanodevices can deliver therapeutic doses to tumors.

### Keywords

radioactive composite nanodevice;  $^{198}\text{Au}$ ; Cancer

### Background

Every year, more than half a million cancer related deaths and approximately 1.3 million new cases [1] are reported in the United States. Radiotherapy has been used in almost all forms of cancers with varying degrees of success. One of the challenges with radiation therapy is the delivery of a lethal dose of radiation to the tumor while leaving the surrounding normal tissue unharmed. Local delivery of radioactive gold has also been successful [2,3]. However, systemic

Corresponding Author: Lajos P. Balogh Ph.D. email: lajos.balogh@roswellpark.org, Ph: 716-845-3886, Fax: 716-845-8254.

**Publisher's Disclaimer:** This is a PDF file of an unedited manuscript that has been accepted for publication. As a service to our customers we are providing this early version of the manuscript. The manuscript will undergo copyediting, typesetting, and review of the resulting proof before it is published in its final citable form. Please note that during the production process errors may be discovered which could affect the content, and all legal disclaimers that apply to the journal pertain.

targeted approaches with tumor directed antibody (or peptide) radiation therapy has been used with limited success, because of the limited activity that can be carried by antibodies.

Targeted drug delivery has been the ultimate goal to treat various diseases. Among others, poly (amidoamine) (PAMAM) dendrimers have been proposed as versatile vehicles of drug transport to specific organs and tissues due to their unique external and internal functionalities that can be altered according to need. These spherical macromolecules have modifiable surface functionalities that offer a multipurpose mode to covalently attach drugs, diagnostic/imaging modules and/or targeting moieties, and allow the control of effective surface charge. However, the expensive starting materials, the required multistep synthesis, and characterization of the multifunctional nanodevices often present a serious challenge.

PAMAM dendrimers are ideal for preparation of composite nanoparticles. These organic-inorganic hybrid nanoparticles are composed of very small and uniformly dispersed inorganic guest domains that are physically trapped within nanoscopic sized organic hosts [4–9]. Using PAMAM dendrimers as templates, composite nanoparticles can be fabricated with precise size, nearly monodisperse distribution, and with well-defined surface charge. By covalently attaching targeting moieties, imaging markers and other functional groups to the composite nanoparticles, composite nanodevices (CNDs) can be constructed that may be used for targeting specific imaging and/or drug delivery. Specific advantage of these nanodevices is that one can change the delivered content without substantially changing the surface, which is exposed to cellular and other biologic interactions. Dendrimer based composite nanodevices (CNDs) display stability and robustness in solutions (including biologic fluids) because of the molecular level mixing of their individual components. A unique advantage of this approach is that appropriate components and properties can be separately selected, developed, optimized, then combined into a nanodevice with regulated size, charge, surface functionality and payload.

PAMAM templates provide a convenient way to create of medical composite nanodevices (CND). The interior and/or the exterior of the dendrimer host can be cationic, anionic, or nonionic, depending on their termini, interior functionalities and pH. The properties of these CNDs allows design and selection of their size and charge, including covalently bound surface functionalities with labeling moieties such as biotin, and with targeting moieties such as peptides [10], or folate and chemotherapeutic agents as methotrexate [11]. To understand the characteristics that govern differential biodistribution in mouse tumor model systems we have also examined the effects of size and charge of these CNDs on their interactions with complex biological systems [12,13]. We have found that the interaction of CNDs with the biological environment (solubility, biocompatibility, biodistribution) is dominated by the surface properties of the host molecule. Charge, size, composition, and 3-D structure are all critical in determining the in vivo biodistribution, and therefore the efficacy of nanodevice imaging and possible therapies.

Using CNDs in radiation medicine is potentially attractive. An analysis of tumor type should allow for the selection a pre-made template and of the appropriate radioactive isotope. The next step is the immobilization of the isotope in a CND, which can then be efficiently delivered to specifically kill tumor cells with minimal collateral damage.

Some of the fundamental problems that can be overcome by the use of targeted CNDs are those of solubility and dose delivery. Many radioisotopes are often practically insoluble in water or body fluids, but may become readily available if trapped in nanodevices of different sizes, contents and surfaces. Use of CNDs permits the delivery of at least a log-fold higher radioactivity than that available with current radioactive antibody therapies. As opposed to labeled antibodies, not only one radioisotope, but 1–1000 atoms can be encapsulated in one dendrimer composite particle [14], thereby one CND can carry multiple radioactive particles

to tumor cells, depending on the chemistry of the encapsulated isotopes. To prove the feasibility of this systemic targeted approach, it has to be first demonstrated that the suggested treatment has the potential to be effective, if the necessary dose is delivered to the tumor. Accordingly, we have tested a nanobrachytherapy approach to treat mouse melanoma by injecting single doses of poly $\{^{198}\text{Au}\}$  nanodevices directly into the tumor. The specific activity of an individual  $\{^{198}\text{Au}\}$  CND particle is in the range of  $1\text{E}-15$  Ci/nanoparticle ( $3.7\text{E}-25$  Bq/nanoparticle), thus individual particles in high dilution should not be harmful, while localization of CNDs at or in the tumor may still deliver a therapeutic dose.

It is well known that the angiogenic tumor microvasculature is very different from the fully formed and normal microvasculature; it is leakier and often lacks pericytes, or has aberrant morphologies [15–18]. The differences between the tumor microvasculature and the normal microvasculature may result in enhanced permeability and retention effect (EPR) [19]. Similar accumulation of macromolecules in the tumor was also found after intravenous injection of an albumin-dye complex (MW=69,000), as well as after injection into normal and tumor tissues. The complex was retained only in tumor tissue for prolonged periods. The Duncan group has shown [20] that higher generation dendrimers and dendrimer/cis-platinum complexes may become trapped in tumor vasculature due to the EPR effect [21]. PAMAM dendrimers have been shown to exhibit different permeability or cellular uptake depending on their size and surface charge. The angiogenic tumor microvasculature is then another exciting target, where nanoparticles are specifically sent through the tumor microvasculature to the tumor, or directly to the microvasculature, using this surface recognition approach [22].

We have studied the biodistribution of both the template PAMAM dendrimers and their respective gold composites ( $\{\text{Au}\}$ ) to establish a baseline for evaluation of their in vivo targeting efficiency. We have found that more of the positively charged nanoparticles were retained in tissues than the neutral or negatively charged nanoparticles. (The term “positively charged” refers to the *surface character* of the polyionic composite particles as shown by the zeta potential of the nanoparticles in dilute aqueous solutions and at physiologic pH values, i.e., between pH=5.5–7.4.) Thus, for the present proof-of-principle demonstration we decided to make and test gold/dendrimer composite nanodevices that are in the size-range of  $d=10$  nm to  $d=50$  nm (to possibly take advantage of the EPR effect) and that are positively charged (to take advantage of the rapid internalization observed for positively charged composite nanoparticles). Using PAMAMs to template composite nanoparticles, the resulting diameter is usually between  $d=3$  and  $d=10$  nm, depending on the generation of the host particle, the surface modifications, and the Au/dendrimer molar ratio [23,24]. However, presently there is no effective method published for the synthesis of positively charged dendrimer composite nanoparticles that are larger than 10 nm. They could be made from larger templates, but synthesis of positively charged large ( $>10$  nm) PAMAM dendrimers, such as amine terminated generation 9 PAMAMs (Mn=467,000,  $d=11.4$  nm) requires a long (9 months) multi-step sequential synthesis that presently results in extremely expensive materials. Synthesis of tecto-dendrimer templates is more practical [25–27], but this method produces methylester or carboxylate terminated (apolar or negatively charged) tecto-dendrimers only as megameric structures [26,27].

Gold-based therapeutic agents have been reviewed recently [28]. Au nanoparticles [29] and nanoshells [30–32] have recently been tested for Photothermal Therapy of cancer. Use of radioactive  $^{198}\text{Au}$ -cluster immunoconjugates (containing 11–33 Au atoms) was reported in the early 90s, but due to the insufficient delivered dose, the research was discontinued [33].

Many attempts have been made to target radionuclides to tumors with the best-known approaches being the use of radiolabeled monoclonal antibody therapy. In the past, radiolabeled antibodies for direct tumor cell targeting have received wide interest for receptor imaging. In

general, however, the penetration of these macromolecules into tumor tissue has been problematic, with typically only 0.001% – 0.01% of the injected dose being localized to each gram of solid human tumor tissue. Several factors account for this poor penetration: (i) antibodies in the circulation must travel across the endothelial cell layer and often through dense fibrous stroma before encountering tumor cells, (ii) the dense packing of tumor cells and tight junctions between epithelial tumor cells hinder transport of the antibody within the tumor mass, (iii) the absence of lymphatics within the tumor contributes to the buildup of a high interstitial pressure which opposes the influx of molecules into the tumor core, (iv) antibodies entering the tumor are absorbed at the perivascular regions by the first tumor cells encountered, leaving none to reach tumor cells at sites further from the blood vessels, and (v) subpopulations of the rapidly mutating tumors can readily lose antigens targeted by the antibodies.

Use of radioactive  $^{198}\text{Au}$  containing nanodevices in treating tumors has not yet been reported in the peer-reviewed literature, We therefore set out to develop methods to synthesize and characterize radioactive composite nanodevices and then test these CNDs in mouse tumor model systems for local control of tumor growth.

To justify the ‘targeted dose delivery with nanocomposites’ approach, first it has to be demonstrated that radioactive composites can be made with sufficient activity, and the treatment will be effective, if the dose is delivered to the tumor. Use of radioactive gold has been approved by the FDA for radiation treatment of tumors.  $^{198}\text{Au}$  ( $t_{1/2}=2.69$  days) decays dominantly by beta-radiation (99%, 0.96 MeV), which has an efficient radius of about 1 mm in tissue. Radioactive gold was used in interstitial brachytherapy for treatment of prostate cancer initially in the form of micron-sized gold colloid particles [2] and later with seed technique [3]. With biopsy results approaching a 80% negative rate, and, at 5 years, a cancer specific survival of 100% for Stages A and B1, 90% for Stage B2, and 76% for Stage C, this form of treatment offers an effective and well-tolerated alternative mode of therapy for patients with localized prostate cancer.

## Materials and methods

### Nomenclature

We identify dendrimers by listing family, core, hierarchy, and termini in their material name according to the following scheme [23]:

DENDRIMER FAMILY\_CoreGeneration#.Terminal group(s)

Thus, PAMAM\_E5.NH2 is an ideal ethylenediamine (EDA or E for short) core generation five poly(amidoamine) (PAMAM) dendrimer with theoretical number of primary and tertiary amines (in this case,  $n=128$  primary amine termini). Subscripts are used to mark measured properties: PAMAM\_E5.(NH2) $_{119\pm5}$  denotes an EDA core G5 PAMAM material that has  $119 \pm 5$  primary amine terminal groups measured.

To describe the complicated structure of dendrimer complexes and composite nanoparticles, we use the following simple convention: brackets denote complexes, while braces represent nanocomposite structures.

Nanocomposites are also named according to the same pattern:

{(Component#1) $_i$ (Component#2) $_j$ ...-FAMILY\_Core.Generation#. (TerminiA) $_m$ (TerminiB) $_n$ ...}

Thus, the formula  $\{(Au^0)_{14.5}\text{-PAMAM\_E4.NH2}\}$  denotes a gold dendrimer nanocomposite in which a generation four amine terminated ethylenediamine core poly(amidoamine) (PAMAM) dendrimer contains 14.5 zerovalent gold atoms per dendrimer molecule on average (not

analyzed for end groups). The above scheme provides a relatively simple but consistent way to identify materials. Additional descriptors may be added to the brackets and braces as subscripts and/or superscripts and parentheses can be embedded into each other, e.g.:  $\{(Au^0)_9-E5.(NH_2)_{119}\}_{250\pm 10, d=22\text{ nm}}$  This symbol denotes a  $d=22\text{ nm}$  aggregate particle composed of  $250\pm 10$  primary gold/dendrimer composite nanoparticle containing 9 gold atoms per dendrimer. When it is trivial, which dendrimer family is used, one may follow the shorter pattern and omit naming the family. For example,  $\{(Au^0)_{10}\text{-PAMAM\_E5.NH}_2\}$  and  $\{(Au^0)_{10}\text{-E5.NH}_2\}$  are equivalent names, when only PAMAMs are used. Polymerization was indicated by using a *poly*- prefix, as is common.

## Synthesis and Characterization of PAMAM Dendrimers

Purification and characterization of PAMAM dendrimers were performed as reported previously [12]. Reagent chemicals acetic anhydride, pyridine, MeOH, HCl, and NaOH were purchased from Aldrich (Milwaukee, WI, USA). HPLC grade solvents were used. PAMAM\_E5.NH<sub>2</sub> and PAMAM\_E3.NH<sub>2</sub> ethylenediamine (EDA) core dendrimers were purchased from Dendritech (Midland, MI, USA) in methanol solution and were further purified by dialysis using reconstructed cellulose membranes (Pierce, molecular weight cut-off 10 kDa) to remove potential small molecular contaminants and trailing generations. The materials were lyophilized then characterized by mass spectrometry, high-performance liquid chromatography (HPLC), polyacrylamide gel electrophoresis (PAGE), <sup>1</sup>H NMR, <sup>13</sup>C NMR, acid-base titration, size exclusion chromatography and capillary electrophoresis (CE) to ensure purity and homogeneity of the final products.

**Size Exclusion Chromatography (SEC)**—Experiments were performed using an Alliance Waters 2690 separation module (Waters, Milford, MA, USA) equipped with a Waters 2487 UV A detector (Waters), a Wyatt Dawn DSP laser photometer (Wyatt Technology, Santa Barbara, CA, USA), and an Optilab DSP interferometric refractometer (Wyatt Technology). Citric acid buffer (0.1 M) with 0.025% sodium azide in water was used as mobile phase. The pH of the mobile phase was adjusted to 2.74 using NaOH and the flow rate was maintained at 1 mL/min. Sample concentration was kept at approximately 2 mg/mL and 100  $\mu$ L was injected for all samples. Molar mass moments of the PAMAM dendrimers were determined using Astra software (v.4.7).

**Potentiometry**—The number of terminal groups of dendrimers was measured by potentiometric titration. Potentiometric titration was carried out manually using a Thermo-Orion 230A pH meter and a Mettler Toledo INLAB 422 pH electrode under the protection of nitrogen. dendrimers (4–6 mg) were dissolved in 3 mL of 0.1 M NaCl solution. These dendrimer solutions were titrated by 0.0951 M HCl to pH around 2.3, followed by back titration to pH 11.3 using 0.1021 M NaOH solution.

**High Performance Liquid Chromatography (HPLC)**—A reversed phase ion-pairing high-performance liquid chromatography was carried out using a system consisting of a System GOLDTM 126 solvent module, a Model 507 autosampler equipped with a 100  $\mu$ L loop, and a Model 166UV detector (Beckman Coulter, Fullerton, CA). A Phenomenex (Torrance, CA) Jupiter 5 $\mu$  C5 silica based HPLC column (250mm $\times$ 4.6 mm, 300  $\text{\AA}$ ) was used for separation. Two Phenomenex Widepore C5 guard columns (4mm $\times$ 3 mm) were also installed upstream of the HPLC column. The mobile phase for elution of PAMAM dendrimers was a linear gradient beginning with 90:10 water/acetonitrile (ACN) at a flow rate of 1 mL/min, reaching 50:50 after 30 min. Trifluoroacetic acid (TFA) at 0.14 wt% concentration in water as well as in ACN was used as counter-ion to make the dendrimer-conjugate surfaces hydrophobic. Analyzed dendrimers were dissolved in the mobile phase (90:10water/ACN). The injection volume in each case was 50  $\mu$ L with a sample concentration of approximately 1 mg/mL and the detection

of eluted samples was performed at 210, 240 or 280 nm. The analysis was performed using Beckman's System GOLDTM *Nouveau* software.

#### **Matrix Associated Laser Adsorption Ionization Time of Flight Mass**

**Spectrometry**—MALDI-TOF spectra were obtained, using a Micromass ToFSpec-2E mass spectrometer. Reflection mode was selected as the operation mode. 10 mg/ml betaindoleacrylic acid in acetonitrile/H<sub>2</sub>O (v/vZ70:30) was used as the matrix. One milligram dendrimer samples were dissolved in 1 ml methanol, and then diluted 50 times by methanol to get a final concentration of 0.02 mg/ml. Equal volumes of 0.02 mg/ml dendrimer solution and matrix solution were well mixed. Then, 1  $\mu$ l solution of the mixture was injected on the spots of target. The matrix was prepared at a concentration of 10 mg/ml in 50% acetonitrile and 50% ethanol.

**Capillary Electrophoresis**—The CE analysis was performed on an Agilent Technologies (Waldbronn, Germany). Unmodified silica capillaries (100 mm ID 678.5  $\mu$ m) were obtained from Polymicro Technologies (Phoenix, AZ, USA). These capillaries had an effective length of 70 cm. All the capillaries had a total length of 78.5 cm and an effective length 70 cm. The capillary temperature was maintained at 40°C (in order to decrease the adsorption of PAMAM dendrimers onto the capillary surface) and separation voltage was kept at 20 kV for all the separations. On-capillary UV diode-array detection was used, operated at wavelengths of 200, 210, 250 and 300 nm. Samples were introduced by hydrodynamic injection at a pressure of 50 mbar. Before initial use, the uncoated, fused-silica capillaries were rinsed with 0.1 M NaOH for at least 15 min, then washed with deionized water (resistivity of 18 M $\Omega$ -cm Milli-Q Plus 185 water purification system, Millipore, Bedford, MA, USA) for 15 min, and then conditioned with the running buffer for an additional 15 min. Before each injection, the capillary was rinsed with a sequence of 0.2 M H<sub>3</sub>PO<sub>4</sub> (5 min) solution, followed by deionized water (5 min), then with the running buffer (5 min). For a silanized capillary, 0.2 M H<sub>3</sub>PO<sub>4</sub> was used for both the daily initialization of the capillary and before each injection; 50 mM phosphate buffer (pH 2.5, Agilent Technologies) was used as running buffer. PAMAM dendrimers possess a large number of amine groups in a relatively small volume of the macromolecule thus they can be considered as a powerful buffer system. When PAMAM dendrimers were directly dissolved in pH 2.5 (50 mM) phosphate buffer, an undesirable pH-change may occur depending on the sample concentration due to the high concentration of amino groups. Hence, first we always adjusted the pH of the aqueous dendrimer solution to pH 2.5 by 0.2 M phosphoric acid to form a salt. Dendrimer salt solutions were then freeze-dried for three days using a Labconco system. The dry PAMAM dendrimer phosphate salts were then dissolved in a calculated amount of pH 2.5 phosphate buffer to give a solution equivalent to  $c = 1$  mg/mL PAMAM at the required pH. As a result of this procedure, every nitrogen atom in the dendrimer molecule is protonated and no aggregation takes place between individual dendrimers.

**Polyacrylamide gel electrophoresis**—PAGE of PAMAM dendrimers was performed using a vertical electrophoresis system (Model FB-VE10-1 FisherBiotech) with a commercial power supply (Model EC135-90; Thermo Electron Corporation), precast 4–20% gradient express gels for PAGE (BioExpress) and Tris-glycine (TG) native (pH = 8.3). Separations typically required 1.5 h min at 200 V. Into each sample well 2  $\mu$ l of a sample solution composed of 2 or 3  $\mu$ l 1 mg/ml PAMAM dendrimer and 2 or 3  $\mu$ l sucrose dye solutions (50% sucrose, 1% methylene blue) was injected. Developed gel was stained with 0.025% Coomassie Blue R-250 in 40% methanol and 7% acetic acid aqueous solution overnight. The gels were destained with 7% (v/v) acetic acid and 5% (v/v) methanol in water.

**Nuclear Magnetic Resonance Spectroscopy**—<sup>1</sup>H and <sup>13</sup>C NMR spectra were collected using a Bruker AVANCE DRX 500 instrument and D<sub>2</sub>O as a solvent.

## Synthesis and Characterization of Gold/Dendrimer composite nanoparticles

Fabrication of PAMAM/gold dendrimer nanocomposites was carried out according to the literature [12] using amine terminated PAMAM hosts. The procedures resulted in positively charged composite nanoparticles containing 3–5% Au. Minor differences between the individual composite nanomaterials (CND-1 through CND-4) are listed in Table 1.

**Irradiation of materials**— $^{197}\text{Au}$  captures neutrons very efficiently because of its large cross-section.  $^{198}\text{Au}$  ( $t_{1/2}=2.69$  days) decays dominantly by beta-radiation (99%, 0.96 MeV) and with a small gamma component (0.98%, 1.1 MeV) into a stable  $^{198}\text{Hg}$  isotope. However, the build-up of activity for any given isotope is a function of several intrinsic factors, including isotopic abundance and neutron cross-section, as well as a series of irradiation parameters, including neutron flux and energy spectrum. Irradiation was performed at the Ford Nuclear Reactor in the Phoenix Memorial Laboratories (Ann Arbor, MI). Samples and standards were irradiated in polypropylene vials for 1 min up to 3 hours, in core-face location 112B, with a nominal thermal neutron flux of  $1\text{E}+11$  while rotating. Following an initial decay of at least 2-days, a 15000 second (live-time) count of gamma activity for  $^{198}\text{Au}$  was recorded for each sample, using a HPGe detector (33% relative efficiency), with a 4 second counting geometry. Because irradiation parameters can vary slightly over time within a range of operating conditions, quantification of the activated isotope is rarely approached through direct calculation. Rather, elemental concentrations are determined through comparison on a weight-ratio basis, from activities (measured as gamma counts-per-second) generated in a standard reference material of known composition, assuming we hold all other parameters constant, including irradiation time, flux, decay time, counting time, and detector geometry. Thus, while the general principles are valid for all the reactors, detailed experimental parameters of the procedure have to be worked out independently for future applications. We determined Au concentrations through direct comparison on a weight ratio basis, with the mean activity generated in four replicates of the NIST (U.S. National Institute of Standards and Technology) Au standard. Gamma- irradiations were performed at the Ford Reactor from a  $^{60}\text{Co}$  source. Gamma dose rates were measured with Reuter-Stokes ion chamber model RS-C4-1606-207, (ser. No: Z-89430), which is calibrated annually by the manufacturer against a NIST source.

**Characterization of  $\{\text{Au}^0\}$  and  $\text{poly}(\{\text{Au}^0\})$  dendrimer composite nanoparticles**— $\{\text{Au}^0\}$  and  $\text{poly}(\{\text{Au}^0\})$  gold/dendrimer composite nanodevices (before irradiation, and after radioactive decay, respectively) have been characterized by UV-visible and fluorescence spectrophotometry, NMR, TEM and Dynamic Light Scattering.

**Dynamic Light Scattering**—Particle size distribution measurements were conducted, using a NICOMP 380 ZLS particle size. Zeta potential measurements were calibrated by  $d=200$  nm polystyrenesulfonate standards, Duke Scientific, for which  $\zeta=-40-42$  mV was found consistently.

**Spectroscopy**—UV-Vis spectra were obtained using a Perkin-Elmer Lambda 20 UV-Vis spectrophotometer over the spectral range of 190–1000 nm in 1 cm quartz cuvettes. Fluorescence spectra were measured using a Fluoromax 3 spectrofluorometer and 1 cm quartz cuvettes.

**Transmission Electron Microscopy**—Images were collected, using a JEOL 2010F analytical TEM operated at 200 kV. Specimens were prepared by mounting a drop of aqueous solution of nanoparticles on carbon-coated copper grids and allowing it to dry in air.

**Therapy Experiment**—The animal work was conducted in the animal facility at University of Michigan Medical Center, Ann Arbor, MI, in accordance with federal, local and institutional

guidelines. Eight-week old male C57BL/6J mice (Jackson Labs, Bar Harbor, ME) were caged in a specific pathogen free barrier facility as groups of five or less, and fed *ad libitum* with Laboratory Autoclavable Rodent Diet 5010 (PMI Nutrition International, St. Louis, MO). For treatments the mice were randomly sorted into three groups (A, B and C) of seven mice each, with average tumor volumes in each group ranging from  $438 \pm 114 \text{ mm}^3$  to  $527 \pm 111 \text{ mm}^3$ . The mice were anesthetized via inhalation of isoflurane and the three groups of mice were administered the different treatments. All treatments were intra-tumoral with the dosage delivered to two different areas of the tumor - typically at the 'North' and 'South' poles of the tumor. Mice in Group A were injected with  $35.4 \text{ } \mu\text{Ci}$  ( $75 \text{ } \mu\text{l}$  of  $0.931 \text{ mg/ml}$  solution in PBS) of  $\text{poly}\{^{198}\text{Au}\}_{d=22\text{nm}}$  (CND-4\*) each, while Group B received  $74.4 \text{ } \mu\text{Ci}$  ( $120 \text{ } \mu\text{l}$  of  $0.931 \text{ mg/ml}$  solution in PBS) of  $\text{poly}\{^{198}\text{Au}\}_{d=22\text{nm}}$  (CND-4\*\*) per mouse and Group C was treated with  $75 \text{ } \mu\text{l}$  of phosphate buffered saline (PBS) per mouse.

In a separate experiment, two groups of ten mice each, bearing tumors, were intratumorally injected with either  $120 \text{ } \mu\text{l}$  solution of non-radioactive  $\text{poly}\{^{197}\text{Au}\}_{d=22\text{nm}}$  (CND-4\*\*), corresponding to the original sample having  $74 \text{ microCi}$  activity), or  $120 \text{ } \mu\text{l}$  of PBS. The mice in all groups were observed for eight days after which they were euthanized. If minor ulceration of tumor was seen, the tumor was treated with betadiene. Mice were weighed and their tumors measured on Days 0 (day of treatment), 2, 4, 6 and 8. On Day 6 one mouse from Group B died due to severe ulceration of tumor.

**Tumor Cell Line**—The maintenance of the isogenic B16F10 melanoma cell line by serial passage every two weeks, within C57BL/6J mice was described previously.<sup>13,34</sup> Freshly isolated B16F10 tumor cells from carrier mice were injected subcutaneously into the dorsal surface of eight-week old C57BL/6J mice. The tumors were allowed to grow for about 10 days up to an average tumor volume of  $500 \text{ mm}^3$  (volume = longest diameter  $\times$  shortest diameter<sup>2</sup>  $\times$  0.52).

**Statistical Analysis**—A gaussian linear regression model (SAS PROC MIXED, SAS Institute, Cary, NC) was fit to the initialized logarithm of the tumor volumes between days 2 and 8. The log volumes were initialized by subtracting the log of the day-0 volumes. (We did not include day-0 volumes because the treatments were administered on day 0, and no effects were expected until the second day.) Separate intercepts and slopes for each of the four treatment groups were used as predictors in the model. A first order autoregressive correlation structure was used in the model to account for correlation within mouse over time. The mean growth rates for each of the four treatment groups were estimated. Pairwise differences between the mean group growth rates were computed and tested for significant difference from zero using t-statistics.

## Results and discussion

A fabrication of  $\{\text{Au}0\}$  gold composite from dendrimer templates involves three chemical steps: (a) formation and (b) decomposition of the dendrimer-amine-  $[\text{AuCl}_4]^-$  complex salt, followed by (c) reduction of  $\text{Au}^{3+}$  ions to  $\text{Au}^0$ . Hydrolysis of  $[\text{AuCl}_4]^-$  is a complex process [35] that readily occurs in aqueous solutions of PAMAMs as the nitrogen ligands neutralize HCl, the hydrolysis byproduct. Reduction is usually performed either by adding external reducing agents such as  $\text{N}_2\text{H}_4$  [4] or  $\text{NaBH}_4$  [6], or by utilizing the reductive nature of terminal groups of PAMAMs [36,37]. Reduction of  $\text{Au}^{3+}$  ions by the PAMAM itself may be accelerated by applying UV-irradiation [38]. We have found that the combination of neutron and gamma irradiation induces both  $^{198}\text{Au}^0$  formation and crosslinking of the organic matrix. Based on this observation a novel and simple procedure was developed to fabricate radioactive  $\text{poly}\{^{198}\text{Au}(0)_n\text{-PAMAM}\}$  positively charged  $\{\text{Au}\}$  gold/dendrimer composite nanoparticles in discrete sizes –up to  $d=30 \text{ nm}$ .



## Synthesis of radioactive poly{ $^{198}\text{Au}^0$ } composite nanodevices

There are essentially two ways to create radioactive gold/dendrimer composites, either by activating the topologically trapped gold metal clusters into  $^{198}\text{Au}$ , or by using radioactive [ $^{198}\text{AuCl}_4$ ] $^-$ . After successful scouting experiments, we focused on the first method, because it allowed us to readily characterize the materials both before and after activation. Doses were based on preliminary calculations, presuming the need of 4 microCi of  $\{^{198}\text{Au}\}$  for each tumor (it was assumed that the CNDs are distributed equally through the tumor, and we needed to achieve a dose rate of 0.2 Gy/h). Typical injected amounts in the biodistribution experiments [12] were 50 microgram polymer per mouse, with a typical concentration of  $\text{Au}^0 = 5.0\%$  w/w. Therefore, 2.5 microgram Au should have at least 4  $\mu\text{Ci}$  activity, and the estimated specific activity should be around 1.6 mCi/mg.

Polymerized nanocomposite particles were made by irradiating either the dendrimer-tetrachloroaurate salts or the gold composite nanoparticles in polypropylene containers. PAMAM-tetrachloroaurate salts were prepared in water, as described in the literature [5,14,23].  $\{(\text{Au}^0)_n\text{-PAMAM\_E5.NH}_2\}_{d=5\text{nm}}$  composite nanoparticles were fabricated from PAMAM dendrimers and  $\text{HAuCl}_4$  [12,39].

Activation of gold and crosslinking of the dendrimer templates can be achieved either in solid form or in aqueous solutions. First, we exposed pre-made composite samples (CND-1) in solid form to simultaneous neutron and gamma-radiation in the Phoenix nuclear reactor (see material section). Our specific target activity – based on calculations considering typical radiation doses – was 1.6  $\mu\text{Ci}/\text{mg}$ . Although we achieved the necessary radioactivity, the materials became insoluble in water after irradiation.

Next, the organic host was irradiated by only gamma rays (from a  $^{60}\text{Co}$  source). The target exposure for these PAMAM dendrimers was chosen to correspond to the gamma-exposure that CND-1 received in the reactor in the previous experiment. After irradiation of 200 mg samples for 51, 102 and 153 min (i.e., with 64, 128 and 193 Mrad doses) respectively, these materials have also become insoluble in water. Only trace amounts of the original PAMAMs remained soluble, the PAGE analysis of which clearly showed signs of crosslinking, i.e., the originally distinctive spots now indicated a considerably broadened Mw distribution and molecular mass increase (not shown).

Next, we irradiated dilute aqueous solutions of CND-2 gold nanocomposite samples as a function of time. Size and size distribution of the resulting polymeric composite nanoparticles were unaffected when the samples were irradiated with low doses and in solution. In these experiments activation of  $^{197}\text{Au}$  to  $^{198}\text{Au}$  occurred (neutron capture efficiency is around 50% of the theoretically targeted value [22]). Under the described conditions partial crosslinking (“radiation polymerization”) of the organic component in the nanoparticles was also observed for irradiations longer than 10 minutes. We have studied the empirical correlation between particle diameter and irradiation time using pre-made composites dissolved in water. These solutions (CND-2) were irradiated in polypropylene containers for up to 3 hours. Irradiation up to two hours increased the amount of radioactive gold in the composite and simultaneously partially crosslinked the hosts into spherical radioactive particles, which remained soluble. Table 2 shows a representative set of data of diameters (volume weighted averages of the dominant peaks) as a function of irradiation time. *Poly*{ $\text{Au}^0$ } composite nanoparticles typically display multimodal, but distinct distributions in solutions, which is illustrated in Figure 2. DLS data (Table 3) suggest that the product (similarly to silver/dendrimer composites [10]), is dominantly composed of polymerized primary composite nanoparticles and a small amount of aggregates.

Broadened peaks in the  $^1\text{H}$  NMR spectra (Figure 3) indicate the polymeric nature of the partially crosslinked PAMAM hosts. The exact mechanism is yet unknown. We speculate that radical mechanisms (that are usually responsible for beta-alanine crosslinking), as well as local heat effects (that are known to result in retro-Michael reaction causing a rearrangement of the molecular structure [40]) may be responsible.

The resulting CNDs preserve their net positive charge, although the measured zeta potential values (Table 2) are approximately half of what has been found for the starting materials, for which the zeta potential was around +40 mV. Decrease of surface positive charge indicates involvement of primary amine terminal groups in the ensuing polymerization reactions during radiation polymerization. However, the net positive zeta-potential indicates the existence of primary amine functions on the surface of the particles.

Samples irradiated for longer than 2 hrs precipitated from the solvent. Long irradiation times (high doses) always resulted in insoluble composite materials.

It is well known that the majority of surface plasmon resonances of noble metal nanocrystals in the UV-vis spectrum shifts towards longer wavelengths (from red to blue, i.e., lower energies) when particles aggregate [41,42]. However, UV-visible spectra of the plasmon peaks due to gold clusters (at 520 nm) in the polymerized composite particles are practically the same before and after irradiation (Figure 4) indicating that the Au nanoclusters did not coalesce during polymerization. (Insoluble samples also showed the characteristic red color of gold colloids).

Size and size distribution of the resulting polymeric composite nanoparticles were unaffected when the samples were irradiated with low doses and in solution. At medium levels, partial crosslinking occurred and larger, but still spherical structures formed (“polymerized nanoparticles”). Knowing that the melting point of the PAMAM matrix is between 20 and 34 C, we speculate that the mechanism of formation must include simultaneous melting and crosslinking of the organic matrix. To estimate how many primary particles form a polymerized particle we assumed complete space-filling (100% packing, due to melting of the organic matrix). Then, a volume of one poly-CND particle with a diameter of 29 nm would be equal to the volume of 195  $\{\text{Au}^0\}_{d=5\text{nm}}$  CND particles. We have also observed the presence of a few large aggregates of these poly-CND particles both by TEM and DLS. Such an aggregate contains  $\text{poly}\{\text{Au}^0\}$  composite nanoparticles connected by their surfaces possibly by H-bonding. The packing density of this spherical aggregate was estimated as 50%. Thus, a  $d=205$  nm aggregate particle composed of  $d=22$  nm  $\text{poly}\{^{198}\text{Au}_n\}_{d=22\text{nm}}$  particles would contain 54  $\{^{198}\text{Au}_n\}_{d=22\text{nm}}$  polymerized nanoparticle per aggregate by volume comparison.

Structure of these polymerized composite particles are supramolecular hybrid networks that resemble to other supramolecular architectures, such as “megamers” suggested by Tomalia [26,27]. However, megamers” are structure-controlled, higher-complexity entities, while polymerized composite nanoparticles are not structure-controlled yet, although do represent a higher complexity. They also form through a random process, probably by radical polymerization – the exact mechanism is yet unknown.

### Tumor Radiation Therapy

For therapy experiments, level of gold activation and polymerization of the dendrimer components were controlled by setting the irradiation time and dose within the timeframes and concentrations identified above. We used a modified experimental setup (water cooling) during irradiation to avoid thermal shock of nanocomposite sample (CND-4) due to gamma heating. The specific activities of irradiated nanomaterials were 0.472  $\mu\text{Ci}/\text{mg}$  (CND-4\*) and 0.632  $\mu\text{Ci}/\text{mg}$  (CND-4\*\*) respectively.

In the first experiment, we injected intratumorally three separate groups of seven mice with a single dose of  $\{^{198}\text{Au}\}$  in PBS: group A with 35  $\mu\text{Ci}$  (CND-4\*), group B with 74  $\mu\text{Ci}$  (CND-4\*\*), and group C with the PBS control. Growth of the tumors was followed for 8 days (Figure 5, Table 4). Although the 35  $\mu\text{Ci}$  (CND-4\*) dose did show a slower tumor growth compared to untreated tumors, it was not statistically significant ( $p=0.5261$ ). However, for the 74  $\mu\text{Ci}$  (CND-4\*\*) dose we observed a statistically significant ( $p=0.0245$ ) over 45% reduction of tumor growth in the animals when compared to the untreated or 35  $\mu\text{Ci}$  CND-4\* solution ( $p=0.0182$ ). In a second experiment, either PBS (untreated) or “cold”  $\{^{197}\text{Au}^0\}_{d=29\text{ nm}}$  composite nanoparticles (the same as CND-4\*\*, but with decayed radioactivity) were injected into tumors and the growth recorded (Figure 5, Table 4). There was no statistical difference between the tumor growth of untreated animals and the ones treated with cold CND-4\*\* ( $p = 0.7127$ ). These results demonstrate that the 74  $\mu\text{Ci}$  beta radiation carried by composite nanodevices directly into the tumor was sufficient to significantly slow tumor growth and that this was due to the radioactive dose, not to the CND itself. (The fate of radioactively decayed gold nanocomposite particles is presently under investigation.)

This study gives the first successful indication of the possible therapeutic use of radioactive nanodevices when delivered to tumors. The above experiments validates a simple nano-brachytherapy approach, injecting the radioactive CND into the tumor, but it also points out that intravenously injected targeted CND radiation therapy is now a possibility as well. It is typical in systemically targeted (intravenously injected) antibody experiments in mice to inject 300–700  $\mu\text{Ci}$  of dose, often in a fractionated manner, with 5–10% being delivered to the tumors. The 74  $\mu\text{Ci}$  intratumoral dose needed to slow tumor growth indicates is in the range of doses possible for targeted systemic therapies.

The technology described here enables us to encapsulate different radionuclides within devices of defined size and targeting properties, delivering a log fold more radiation dose than previously possible with antibody techniques. An additional advantage of this approach is the opportunity to develop a guided therapy, in which the efficacy of delivery can be confirmed first (imaging stage) and radioactivity delivered to a tumor can be increased either by increasing the number of the guests carried, or by increasing the specific activity of the guest atoms, without destroying the targeting ability of the nanodevice, which is related primarily to the surface of the nanodevice. Additionally, varying the particular nature and specific activity of the guests encapsulated in the nanodevices, will permit the application of imaging techniques from whole animals down to sub-cellular levels using the same nanodevices with appropriate imaging guest contents. These targeted CNDs could be used for image-guided therapy of the tumors. Combination therapies are possible, with CNDs carrying combinations of alpha, beta, or gamma emitters. If radiosensitizers or other cytotoxic agents are added to the CND surface one could have potentially greatly increase tumor kill.

## Conclusion

We have successfully fabricated radioactive gold/dendrimer composite nanodevices in various ( $d=5$ ,  $d=10$ ,  $d=22$  nm, and  $d=29$  nm) sizes.  $Poly\{^{198}\text{Au}^0\}$  nanodevices were synthesized from non-radioactive ( $d=5$  nm) gold/PAMAM composites simultaneously utilizing both the gamma-radiation and the neutron radiation components in the reactor. Increase in size of the composite nanoparticles is due to the partial crosslinking of the PAMAM dendrimers by the combined effect of gamma radiation and heat, while absorption of neutrons activate the gold component to  $^{198}\text{Au}$ . Level of activation and degree of polymerization were manipulated by varying the irradiation time and the neutron/gamma ratio. A single injection of 74  $\mu\text{Ci}$  radioactive  $\{^{198}\text{Au}\}$  composite nanodevice ( $d=29$  nm) in PBS solution directly into the tumor resulted in statistically significant tumor growth retardation (more than a 45% reduction of tumor growth within 8 days) in a melanoma tumor mouse model. Significantly, the dose of radiation needed for the

tumor growth retardation is in the range of doses that could easily be delivered by nano-brachytherapy approaches or by fractionated targeted systemic radiation therapy with activated composite nanodevices.

### Acknowledgments

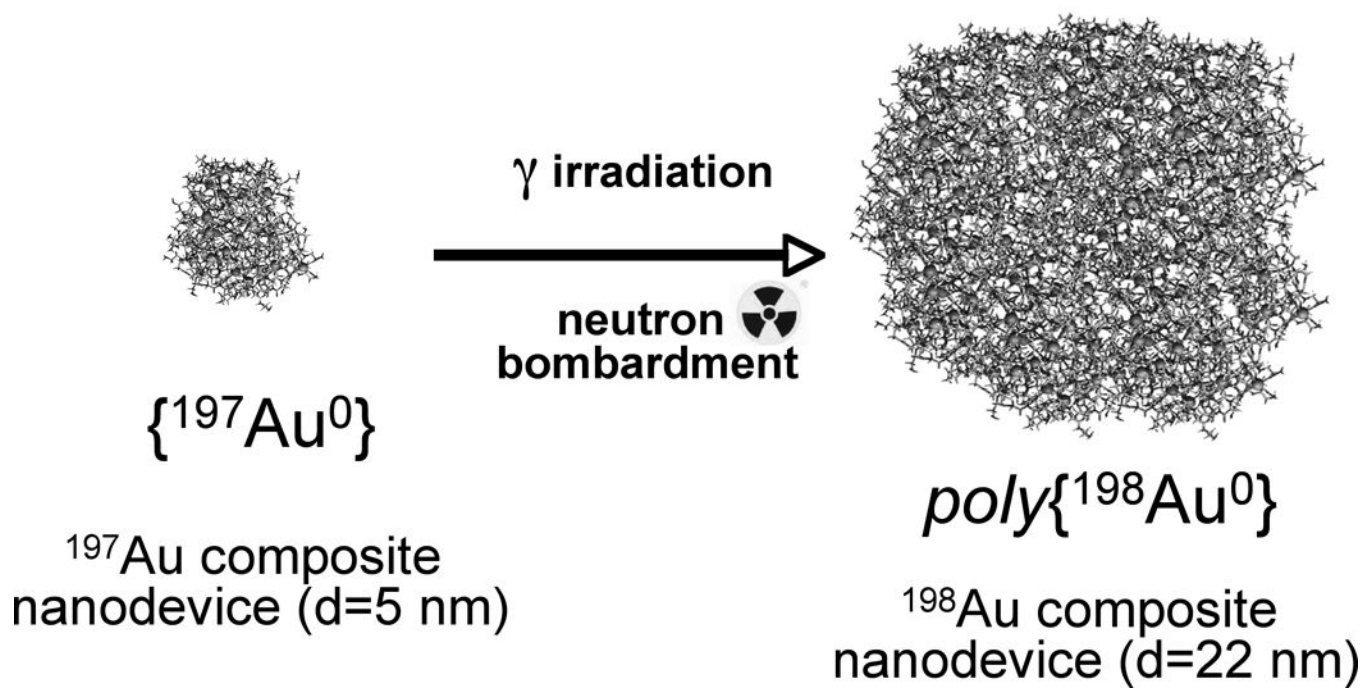
This research was funded with Federal Funds in part from the U.S. Department of Energy (FG01-00NE22943) from the Department of Defense (#DAMD17-03-1-0018), and the National Institutes of Health (NIH)/National Cancer Institute (NCI) (# R01-CA-104479-01).

### References

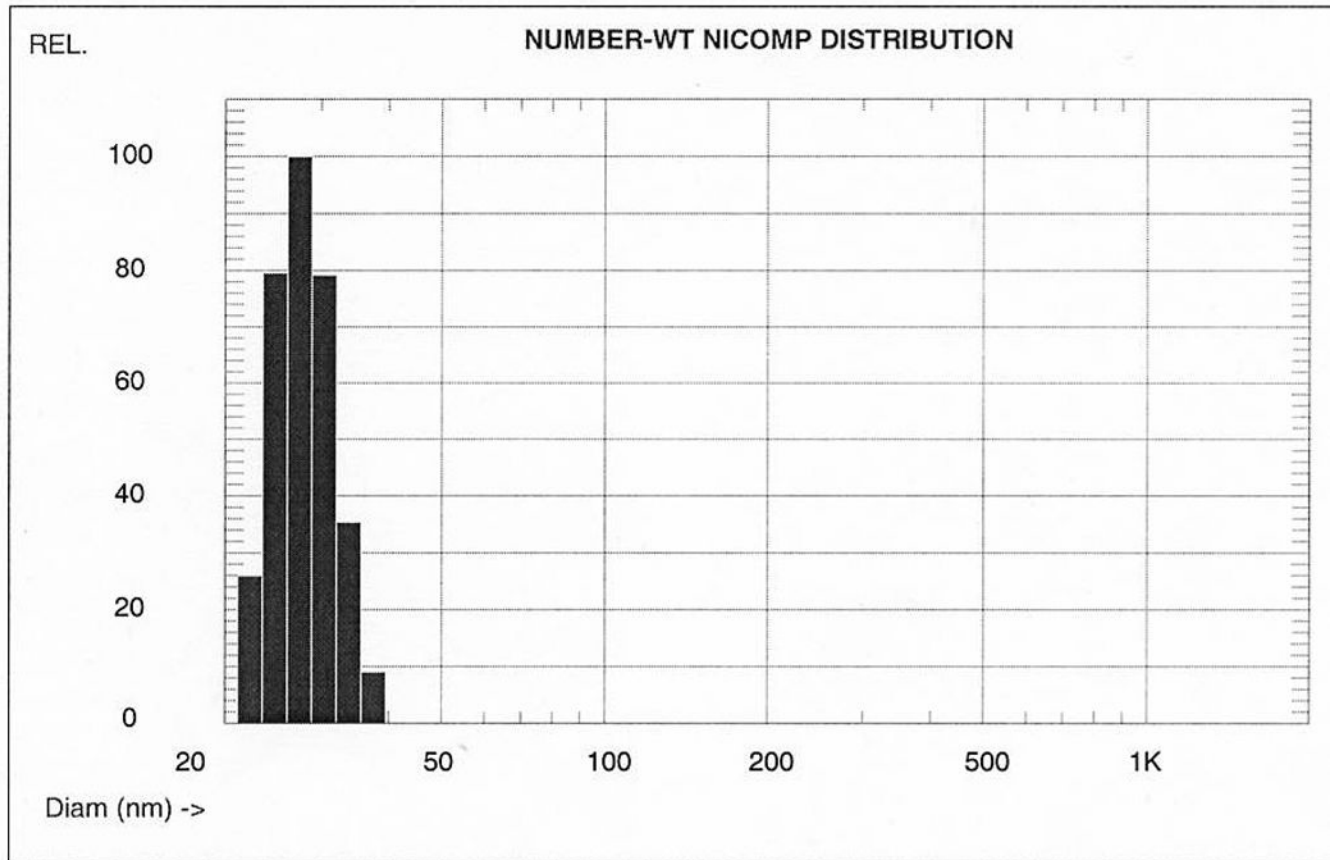
1. Jemal A, Tiwari RC, Murray T, Ghafoor A, Samuels A, Ward E, Feuer EJ, Thun MJ. Cancer Statistics. *Ca Cancer J Clin* 2004;54:8–29. [PubMed: 14974761]
2. Flocks RH, Kerr HD, Elkins HB, Culp DA. Treatment of carcinoma of the prostate by interstitial radiation with radioactive gold: a preliminary report. *Journal of Urology* 1952;68:510–522. [PubMed: 14955881]
3. Loening SA. Gold seed implantation in prostate brachytherapy. *Seminars on Surgical Oncology* 1997;13:419–424.
4. Balogh L, Laverdure KS, Gido SP, Mott AG, Miller MJ, Ketchel BP, Tomalia DA. Organic/Inorganic Hybrid Materials. *Mat. Res. Soc. Symp. Proc* 1999;576:69–75.
5. Esumi K, Suzuki A, Aihara N, Usui K, Torigoe K. Preparation of Gold Colloids with UV Irradiation Using Dendrimers as Stabilizer. *Langmuir* 1998;14:3157–3159.
6. Garcia ME, Baker LA, Crooks RM. Preparation and Characterization of Dendrimer-Gold Colloid Nanocomposites. *Analytical Chemistry* 1999;71:256–258.
7. Tomalia, DA.; Balogh, L. US. 6,664,315 B2. 2003.
8. Tomalia, DA.; Balogh, L. US. 6,995,234. 2006.
9. Balogh L, Tomalia DA, Hagnauer GL. Revolution of nanoscale proportions. *Chemical Innovation* 2000;30:19–26.
10. Lesniak W, Bielinska AU, Sun K, Janczak KW, Shi X, Baker JR, Balogh LP. Silver/Dendrimer Nanocomposites as Biomarkers: Fabrication, Characterization, in Vitro Toxicity, and Intracellular Detection. *Nano Letters* 2005;5:2123–2130. [PubMed: 16277438]
11. Kukowska-Latallo JF, Candido KA, Cao Z, Nigavekar SS, Majoros IJ, Thomas TP, Balogh LP, Khan MK, Baker JR Jr. Nanoparticle Targeting of Anticancer Drug Improves Therapeutic Response in Animal Model of Human Epithelial Cancer. *Cancer Res* 2005;65:5317–5324. [PubMed: 15958579]
12. Khan MK, Nigavekar SS, Minc LD, Kariapper MST, Nair BM, Lesniak WG, Balogh LP. Biodistribution of Dendrimers and Dendrimer Nanocomposites Implications for Cancer Imaging and Therapy. *Technology in Cancer Research & Treatment* 2005;4:603–613. [PubMed: 16292880]
13. Nigavekar SS, Sung LY, Llanes M, El-Jawahri A, Lawrence TS, Becker CW, Balogh L, Khan MK. 3H Dendrimer Nanoparticle Organ/Tumor Distribution. *Pharm. Res* 2004;21:476–483. [PubMed: 15070099]
14. Grohn F, Bauer BJ, Akpalu YA, Jackson CL, Amis EJ. Dendrimer Templates for the Formation of Gold Nanoclusters. *Macromolecules* 2000;33:6042–6050.
15. Folkman, J. Tumor Angiogenesis. In: JF, H., editor. *Cancer Medicine*. 4 ed.. 1. Baltimore: Williams and Wilkens; 1996. p. 181-204.
16. Ribatti D, Vacca A, Dammacco F. The Role of the Vascular Phase in Solid Tumor Growth: A Historical Review. *Neoplasia* 1999;1:293–302. [PubMed: 10935483]
17. Schlingemann RO, Rietveld FJ, Kwaspen F, van de Kerkhof PC, de Waal RM, Ruitter DJ. Differential expression of markers for endothelial cells, pericytes, and basal lamina in the microvasculature of tumors and granulation tissue. *Am. J. Pathol* 1991;138:1335–1347. [PubMed: 1711288]
18. Jain RK. Determinants of Tumor Blood Flow: A Review. *Cancer Research* 1988;48:2641–2658. [PubMed: 3282647]
19. Matsumura Y, Maeda H. A New Concept for Macromolecular Therapeutics in Cancer Chemotherapy: Mechanism of Tumor-tropic Accumulation of Proteins and the Antitumor Agent Smancs. *Cancer Res* 1986;46:6387–6392. [PubMed: 2946403]

20. Duncan R, Malik N, Richardson S, Ferruti P. Polymer Conjugates for anti-cancer agent and DNA delivery Polym, Prepr. Am. Chem. Soc. Div. Polym. Chem 1998;39:180–181.
21. Muggia FM. Doxorubicin-Polymer Conjugates: Further Demonstration of the Concept of Enhanced Permeability and Retention. *Clinical Cancer Research* 1999;5:7–8. [PubMed: 9918196]
22. Balogh LP, Nigavekar SS, Cook AC, Minc L, Khan MK. Development of Dendrimer-Gold Radioactive Nanocomposites to Treat Cancer Microvasculature. *PharmaChem* 2003;2:94–99.
23. Balogh L, Valuzzi R, Laverdure KS, Gido SP, Hagnauer GL, Tomalia DA. Formation of Silver and Gold Dendrimer Nanocomposites. *J. of Nanoparticle Research* 1999;1:353–368.
24. Seo YS, Kim KS, Shin K, White H, Rafailovich M, Sokolov J, Lin B, Kim HJ, Zhang C, Balogh L. Morphology of Amphiphilic Gold/Dendrimer Nanocomposite Monolayers. *Langmuir* 2002;18:5927–5932.
25. Uppuluri S, Swanson DR, Brothers HM, Piehler LT, Li J, Meier DJ, Hagnauer GL, Tomalia DA. Tecto(dendrimer) core-shell molecules: macromolecular tectonics for the systematic synthesis of larger controlled structure molecules. *Polym. Mater. Sci. Eng* 1999;80:55–56.
26. Tomalia DA, Brothers HM 2nd, Piehler LT, Durst HD, Swanson DR. Partial shell-filled core-shell tecto(dendrimers): A strategy to surface differentiated nano-clefts and cusps. *Proc Natl. Acad. Sci. U S A* 2002;99:5081–5087. [PubMed: 11943851]
27. Tomalia DA, Uppuluri S, Swanson DR, Li J. Dendrimers as reactive modules for the synthesis of new structure-controlled, higher-complexity megamers. *Pure Appl. Chem* 2000;72:2343–2358.
28. Shaw IC. Gold-Based Therapeutic Agents. *Chem Rev* 1999;99:2589–2600. [PubMed: 11749494]
29. El-Sayed IH, Huang X, El-Sayed MA. Selective laser photo-thermal therapy of epithelial carcinoma using anti-EGFR antibody conjugated gold nanoparticles. *Cancer Lett* 2006;239:129–135. [PubMed: 16198049]
30. Hirsch LR, Stafford RJ, Bankson JA, Sershen SR, Rivera B, Price RE, Hazle JD, JHN, West JL. Nanoshell-mediated near-infrared thermal therapy of tumors under magnetic resonance guidance. *Proceedings of National Academy of Sciences U S A* 2003;100:13549–13554.
31. Loo C, Lin A, Hirsch L, Lee M, Barton J, Halas N, West J, Drezek R. Nanoshell Enabled Photonics-Based Imaging and Therapy of Cancer Technology in Cancer Research & Treatment. 2004;3:33–40.
32. Loo C, Lowery A, Halas N, West J, Drezek R. Immunotargeted Nanoshells for Integrated Cancer Imaging and Therapy. *Nano Letters* 2005;5:709–711. [PubMed: 15826113]
33. Hainfeld JF, Foley CJ, Srivastava SC, Mausner LF, Feng NI, Meinken GE, Steplewski Z. Radioactive gold cluster immunoconjugates: potential agents for cancer therapy. *International Journal of Radiation Applications and Instrumentation. Part B. Nuclear Medicine and Biology (Oxford)* 1990;17:287–294.
34. O'Reilly MS, Holmgren L, Shing Y, Chen C, Rosenthal RA, Moses M, Lane WS, Cao Y, Sage EH, Folkman J. Angiostatin: a novel angiogenesis inhibitor that mediates the suppression of metastases by a Lewis lung carcinoma. *Cell* 1994;79:315–328. [PubMed: 7525077]
35. Cotton. *Wilkinson Advanced Inorganic Chemistry*. 4 ed.. J. Wiley & Sons; 1980.
36. Esumi K. Dendrimers for Nanoparticle Synthesis and Dispersion Stabilization. *Topics in Current Chemistry* 2003;227:31–52.
37. Lee WI, Bae Y, Bard AJ. Strong Blue Photoluminescence and ECL from OH-Terminated PAMAM Dendrimers in the Absence of Gold Nanoparticles. *J. Am. Chem. Soc* 2004;126:8358–8359. [PubMed: 15237975]
38. Esumi K, Suzuki A, Yamahira A, Torigoe K. Role of Poly(amidoamine) Dendrimers for Preparing Nanoparticles of Gold, Platinum, and Silver. *Langmuir* 2000;16:2604–2608.
39. Bielinska A, Eichman JD, Lee I, Baker JR, Balogh L. Imaging {Au<sup>0</sup>-PAMAM} Gold-dendrimer Nanocomposites in Cells. *J. of Nanoparticle Research* 2002;4:395–403.
40. Tang MX, Redemann CT, Szoka FC. Gene Delivery by Degraded Polyamidoamine Dendrimers. *Bioconjugate Chemistry* 1996;7:703–714. [PubMed: 8950489]
41. Burda C, Chen X, Narayanan R, El-Sayed MA. Chemistry and Properties of Nanocrystals of Different Shapes. *Chemical Reviews* 2005;105:1025–1102. [PubMed: 15826010]
42. Rosi NL, Mirkin CA. Nanostructures in Biodiagnostics. *Chem. Rev* 2005;105:1547–1562. [PubMed: 15826019]

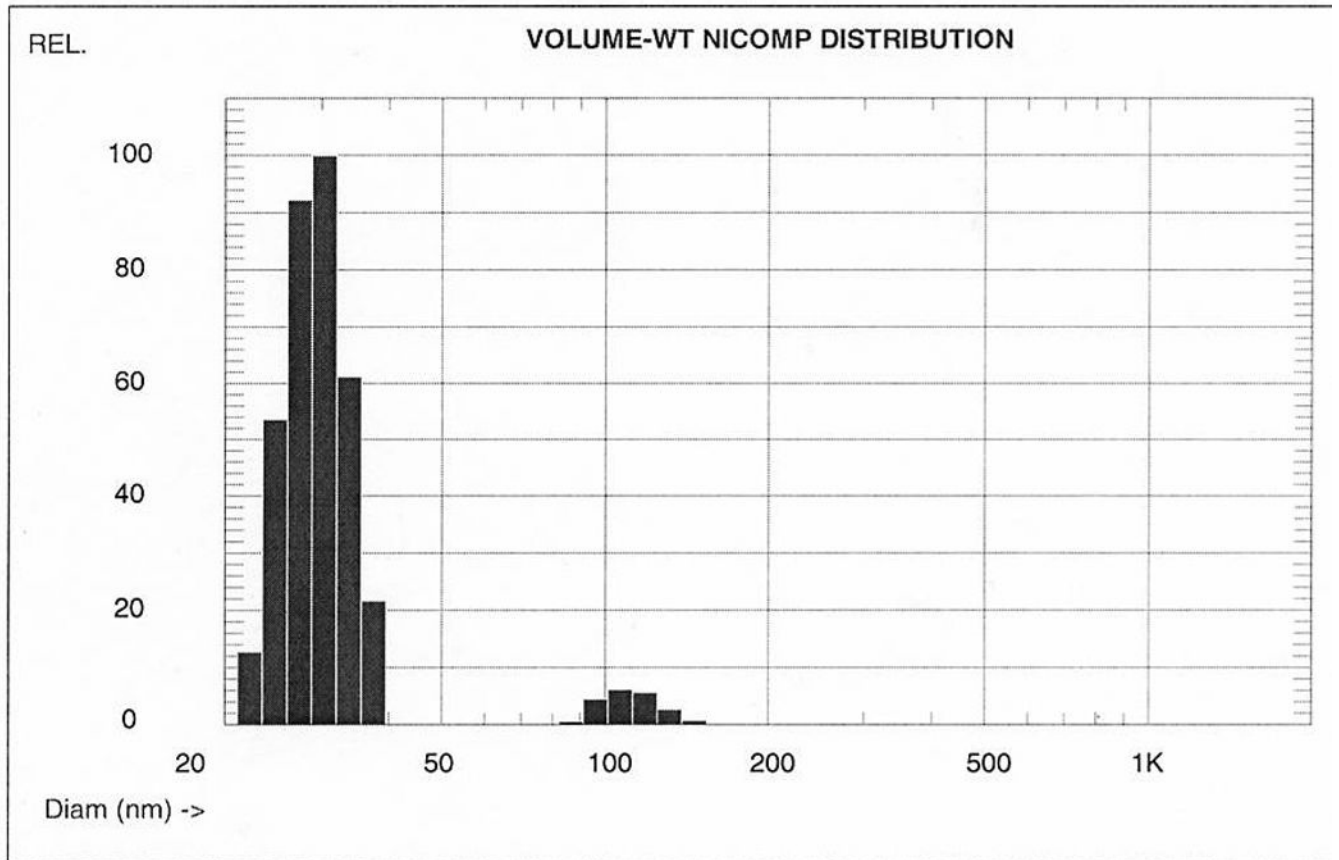
43. Balogh, LP.; Khan, MK. Dendrimer Nanocomposites for Cancer Therapy” Chapter 28: 551–592. In: Amiji, Mansour, editor. Nanotechnology in Cancer Therapy. Boca Raton, London, New York: CRC Press (Taylor and Francis Group); 2006.



**Figure 1.** Schematics of polymerized composite nanoparticle formation through radiation polymerization of the dendrimer network of the templates with simultaneous neutron activation of  $^{197}\text{Au}$  in the gold composite nanoparticles into  $^{198}\text{Au}$ . (Dark dots represent gold atoms and the organic network is grey.)







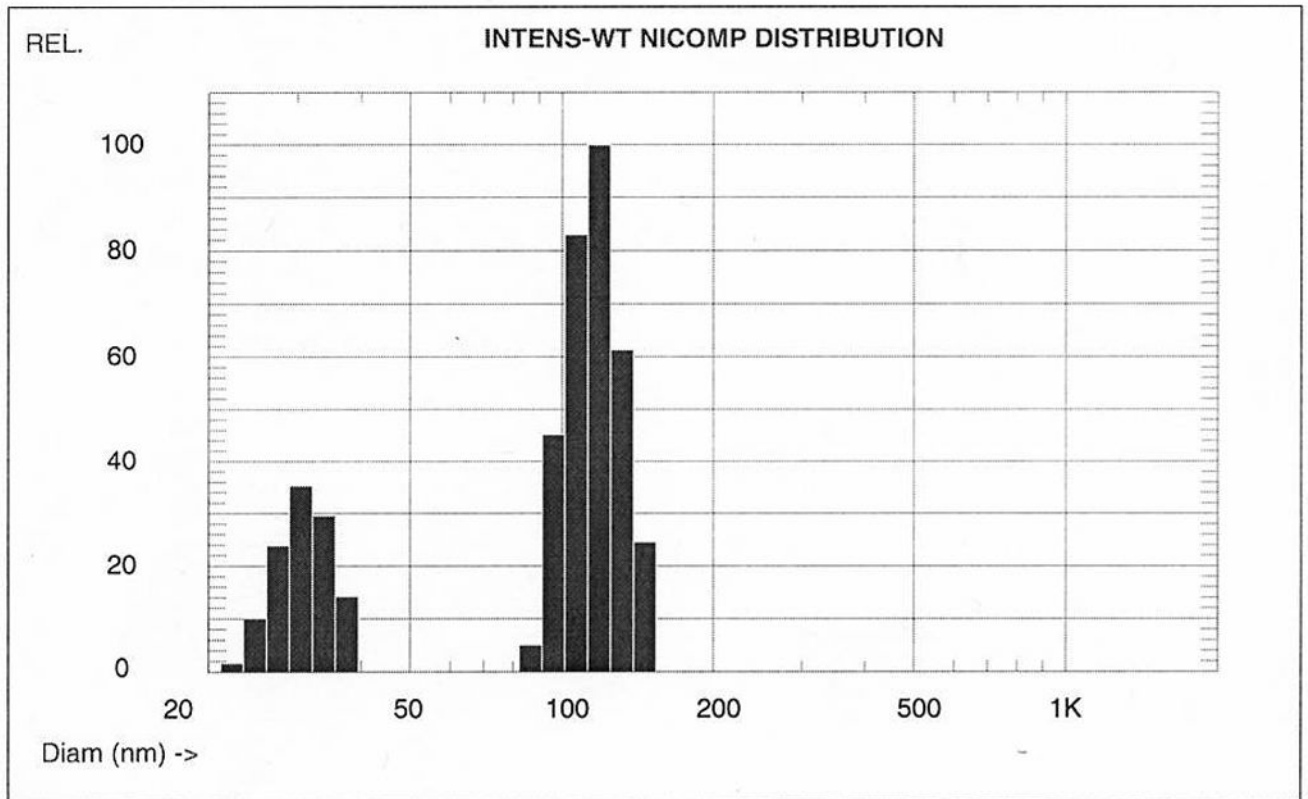


**Figure 2.** Comparison of number, volume, and intensity weighted NICOMP (modified CONTIN) distributions of different composite nanoparticle solutions. Each sample is predominantly composed of single particles of similar size. Volume weighted averages are directly proportional with w/w concentrations (for chemistry calculations), but interaction with biologic objects (e.g., cells) is primarily determined by the number weighted averages, i.e., the number of interacting objects.

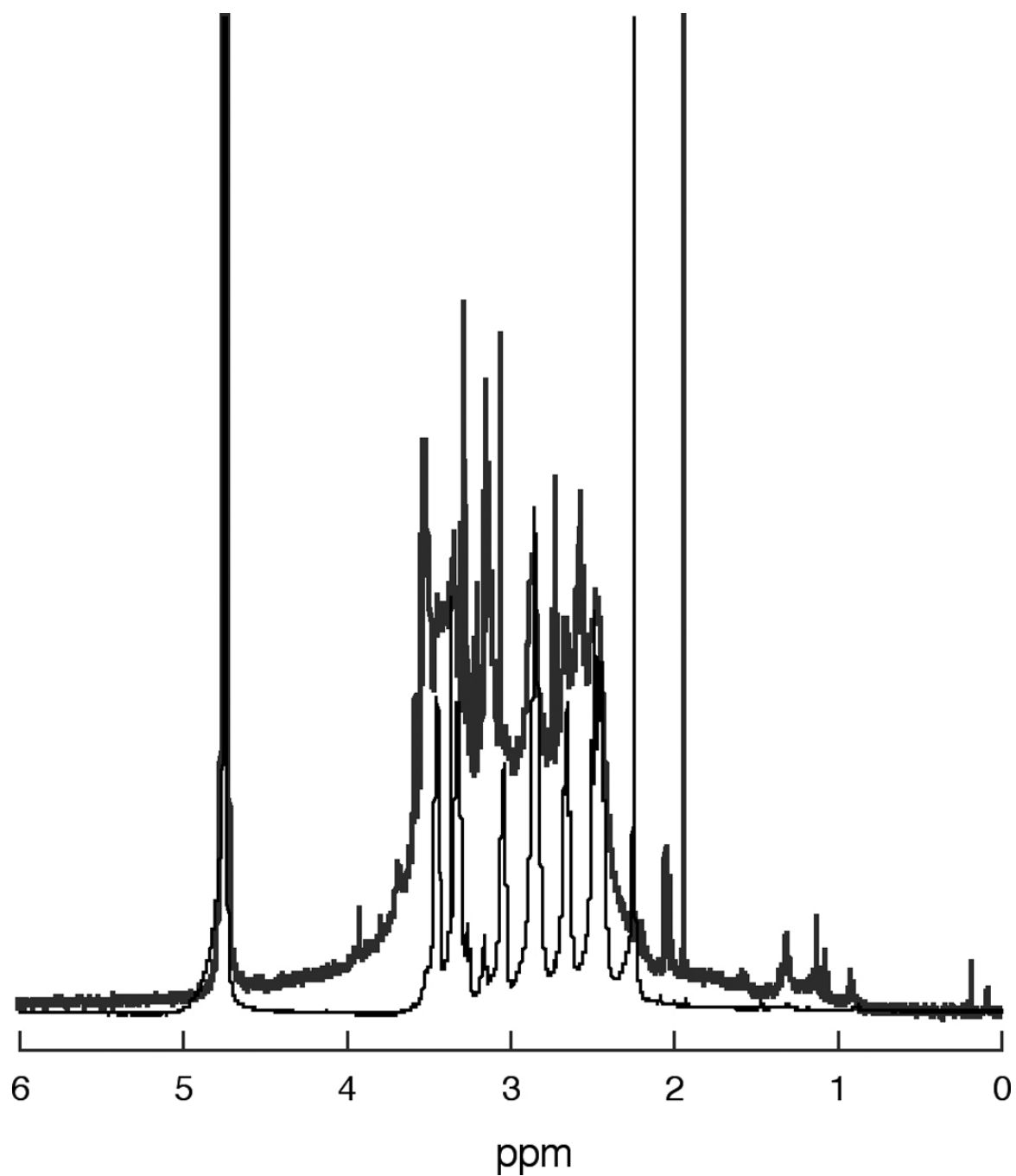


**Figure 3.** Comparison between the  $^1\text{H}$  NMR spectra of the host PAMAM\_E5.NH<sub>2</sub> dendrimer (thin lower line) of and that of the polymerized nanoparticle CND-4\* (thick upper line).

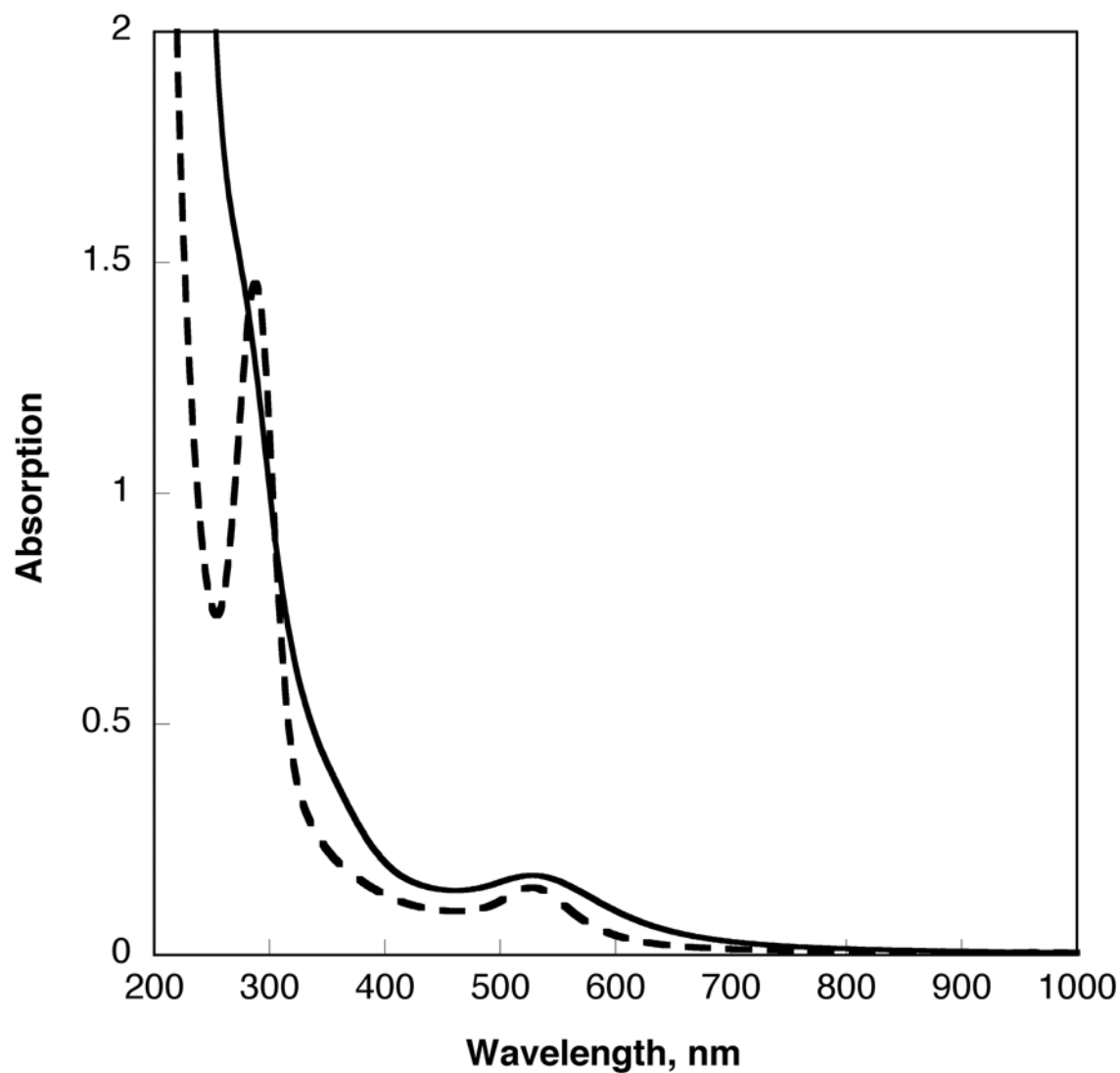


**Figure 4.** Comparison of UV-visible spectra of gold/dendrimer nanocomposite particles (irradiated in water at 25 mg/mL concentration) before ( $\{(Au^0)_{6.53}\text{-PAMAM\_E5.NH}_2\}$ , continuous line) and after radiation polymerization ( $poly\{(Au^0)_{6.53}\text{-PAMAM\_E5.NH}_2\}$ , staggered line) in water, at  $c=1$  mg/ml.

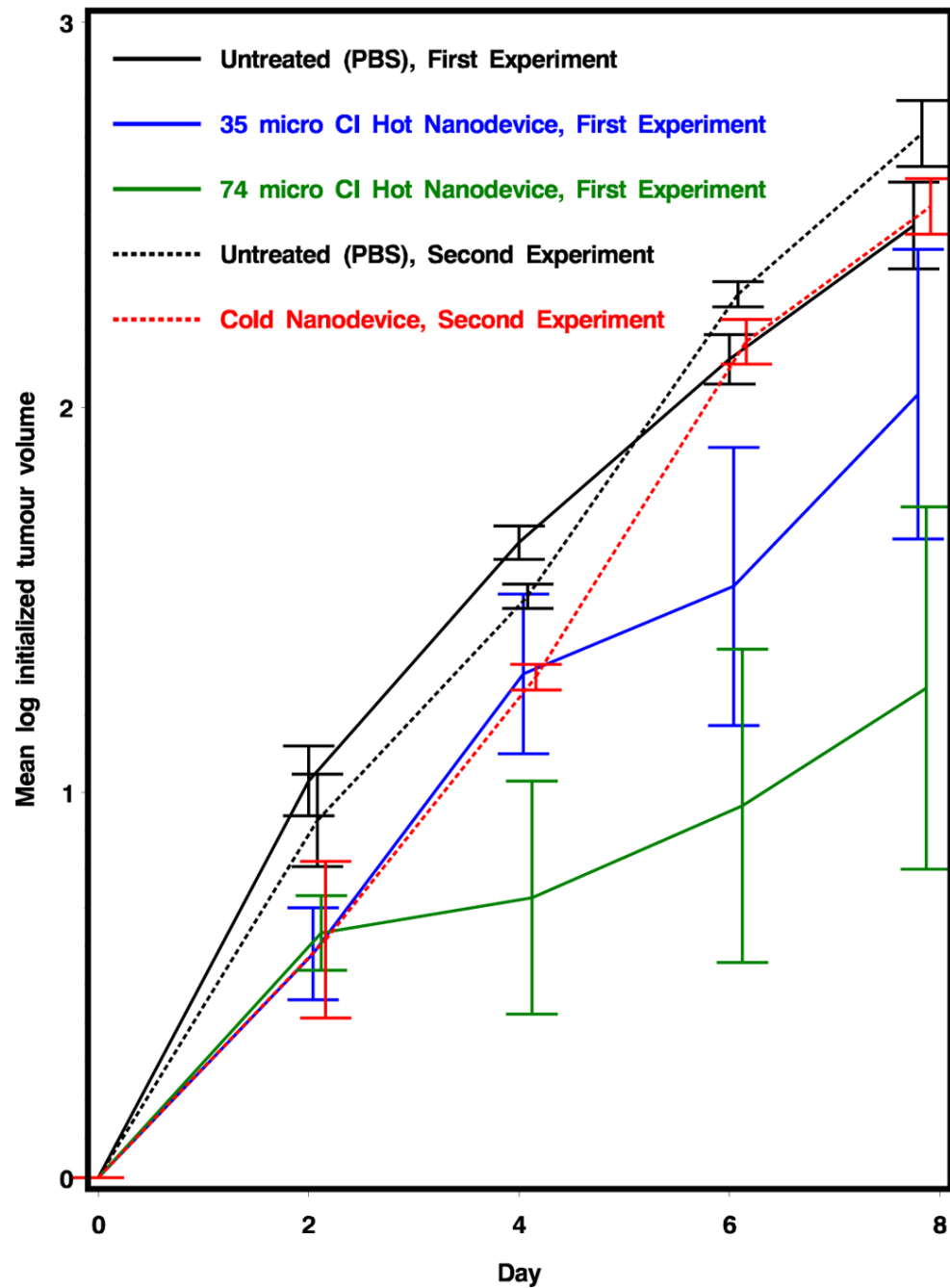


**Figure 4.** Tumor growth of radioactive {Au} CND treated mice versus PBS treated control mice. Error bars represent standard deviation. In the first experiment, groups of mice were administered PBS, 35  $\mu\text{Ci}$  of  $\{^{198}\text{Au}\}$  (CND-4\*) and 74  $\mu\text{Ci}$  of  $\{^{198}\text{Au}\}$  (CND-4\*\*). In the second experiment, mice were administered PBS and CND-4\*\* sample that has been radioactively decayed. Preliminary analysis of this data was shown in our recent book review chapter [43], but the full presentation of data and analysis is now presented here.

**Table 1**

Identification of materials used in the paper. CND-4\* and CND-4\*\* were prepared by irradiating aliquots of CND-4 for different times.

Short notation	Particle Composition
CND-1	$poly\{(Au^0)_{1.75}\text{-PANUM-E3.NH}_2\}$
CND-2	$poly\{(Au^0)_{5.69}\text{-PAMAM\_E5.NH}_2\}$
CND-3	$poly\{(Au^0)_{6.53}\text{-PAMAM\_E5.NH}_2\}$
CND-4	$\{(Au^0)_{5.76}\text{-PAMAM\_E5.NH}_2\}_{d=5nm}$
CND-4*	$poly\{(^{198}Au^0)_{5.76}\text{-PAMAM\_E5.NH}_2\}_{d=22nm}$
CND-4**	$poly\{(^{198}Au^0)_{5.76}\text{-PAMAM\_E5.NH}_2\}_{d=29nm}$

Particle size distributions of soluble *poly* {<sup>198</sup>Au} CNDs after irradiation (NICOMP data-analysis). Sample CND-2A was kept as a control and was not irradiated, while samples E, F and G polymerized and became insoluble in water. The NICOMP distribution model was used to evaluate the bimodal distributions of the {Au} CNDs: peak#1 refers to the composite nanoparticles and peak#2 refers to their (physical) aggregates.

Table 2

Sample CND-2	Volume weighted			Number weighted			Irradiation time (hours)	Zeta Potential (mV)
	Mean diameter (nm)	Std. Dev. (nm)	Percentile	Mean diameter (nm)	Std. Dev. (nm)	Percentile		
2B-peak#1	14.0	1.9	99.4	13.4	1.4	100	1.0	+23.3
2B-peak#2	453	45.1	0.6	0	0	0		
2C-peak#1	16.6	1.7	94.6	15.8	1.9	99.9	1.5	+22.7
2C-peak-2	73.6	10.3	5.4	70.4	6.2	0.1		
2D-peak-1	21.1	2.9	91.2	20.2	2.2	99.9	2.0	+25.2
2D-peak-2	111.2	17.2	8.8	104.9	4.0	0.1		

With permission.43

Table 3

NICOMP size-distribution data for  $poly\{(Au^0)_{5,7,6}\text{-PAMAM}_E5.NH2\}_{d=29nm}$  (CND-4<sup>\*\*\*</sup> nanocomposite after radioactive decay).

Sample	Number Weighted		Volume Weighted		Intensity Weighted	
	Mean diameter nm	Percent %	Mean diameter nm	Percent %	Mean diameter nm	Percent %
CND-4 <sup>***</sup>	27.7	99.9	29.7	94.1	31.0	26.2
Peak 1						
Peak 2	106.4	0.1	110.4	5.9	116.9	73.8



**Table 4**

Estimated differences in growth rates between days 2 and 8 (Mixed Procedure)

Experiment 1						
Label	Estimate	Standard Error	DF	t-Value	P> t	
PBS vs. 35 $\mu$ Ci CND-4*	-0.00403	0.06122	55	-0.07	0.5261	
PBS vs. 74 $\mu$ Ci CND-4**	0.1261	0.06264	55	2.01	0.0245	
35 $\mu$ Ci CND-4* vs. 74 $\mu$ Ci CND-4**	0.1302	0.06066	55	2.15	0.0182	
Experiment 2						
Label	Estimate	Standard Error	DF	t-Value	P> t	
Untreated vs. Cold CND-4**	-0.01969	0.03427	14	-0.57	0.7127	